Electronic Supplementary Material (ESI) for Soft Matter.

Supporting Information for:

High – χ, low – N Micelles from Partially Perfluorinated Block Polymers

Eric R. Williams[1], Wessel van den Bergh[1], and Morgan Stefik[1*]

[1]Department of Chemistry and Biochemistry, University of South Carolina, Columbia, South Carolina, 29208, United States

*morgan@stefikgroup.com

Table S1. Citations for Scheme 1 including the χN values used and the relevant citation. Here, the relevant χ value is $\chi_{core\text{-}solvent}$.

N	χN	Symbol	Border Color	Citation
11	321	Star	Blue	This Work
8	233	Square	Blue	This Work
63	403	Circle	Blue	*Langmuir* **2018**, *34*, 5738 – 5749
63	676	Circle	Blue	*Langmuir* **2018**, *34*, 5738 – 5749
80	849	Circle	Blue	*Small* **2019**, *15*, 1900393 – 1900493
96	614	Circle	Blue	*Soft Mater* **2019**, *15*, 5193 – 5203
278	142	Circle	Blue	*Chem. Mater.* **2016**, *28*, 1653 – 1667
85	2526	Circle	Blue	*Nanoscale* **2017**, *9*, 1393 – 1397
73	255	Circle	Blue	*Macromolecules* **2003**, *36*, 953 – 955
250	35	Diamond	Black	*Macromolecules* **2011**, *44*, 3594 – 3604
400	56	Diamond	Black	*Macromolecules* **2011**, *44*, 3594 – 3604
250	18	Diamond	Black	*ACS Macro Lett.* **2012**, *1*, 982 – 985
400	28	Diamond	Black	*ACS Macro Lett.* **2012**, *1*, 982 – 985
169	123	Diamond	Black	*Macromolecules* **2016**, *49*, 9542 – 9552
169	112	Diamond	Black	*Macromolecules* **2016**, *49*, 9542 – 9552
169	101	Diamond	Black	*Macromolecules* **2016**, *49*, 9542 – 9552
169	90	Diamond	Black	*Macromolecules* **2016**, *49*, 9542 – 9552
246	162	Diamond	Black	*Macromolecules* **2016**, *49*, 9542 – 9552
246	148	Diamond	Black	*Macromolecules* **2016**, *49*, 9542 – 9552
246	130	Diamond	Black	*Macromolecules* **2016**, *49*, 9542 – 9552
373	198	Diamond	Black	*Macromolecules* **2016**, *49*, 9542 – 9552
269	38	Diamond	Black	*Macromolecules* **2018**, *51*, 3563 – 3571
250	35	Diamond	Black	*Macromolecules* **2018**, *51*, 3563 – 3571
403	141	Diamond	Black	*Macromolecules* **2020**, *53*, 417 – 426
403	131	Diamond	Black	*Macromolecules* **2020**, *53*, 417 – 426
90	99	Diamond	Blue	*Macromolecules* **2021**, *54*, 4738 – 4746
59	207	Circle	Blue	*Nat. Commun.* **2013**, *5*, 3599 – 3609
9*	64	Diamond	Blue	*Soft Matter* **2012**, *8*, 623 – 626
12*	179	Diamond	Blue	*Soft Matter* **2012**, *8*, 623 – 626
15*†	232	Diamond	Blue	*Soft Matter* **2012**, *8*, 623 – 626

*Considering ethylene (CH_2CH_2) as the repeat unit

†Contains conflicting information about micelle persistence and was omitted.

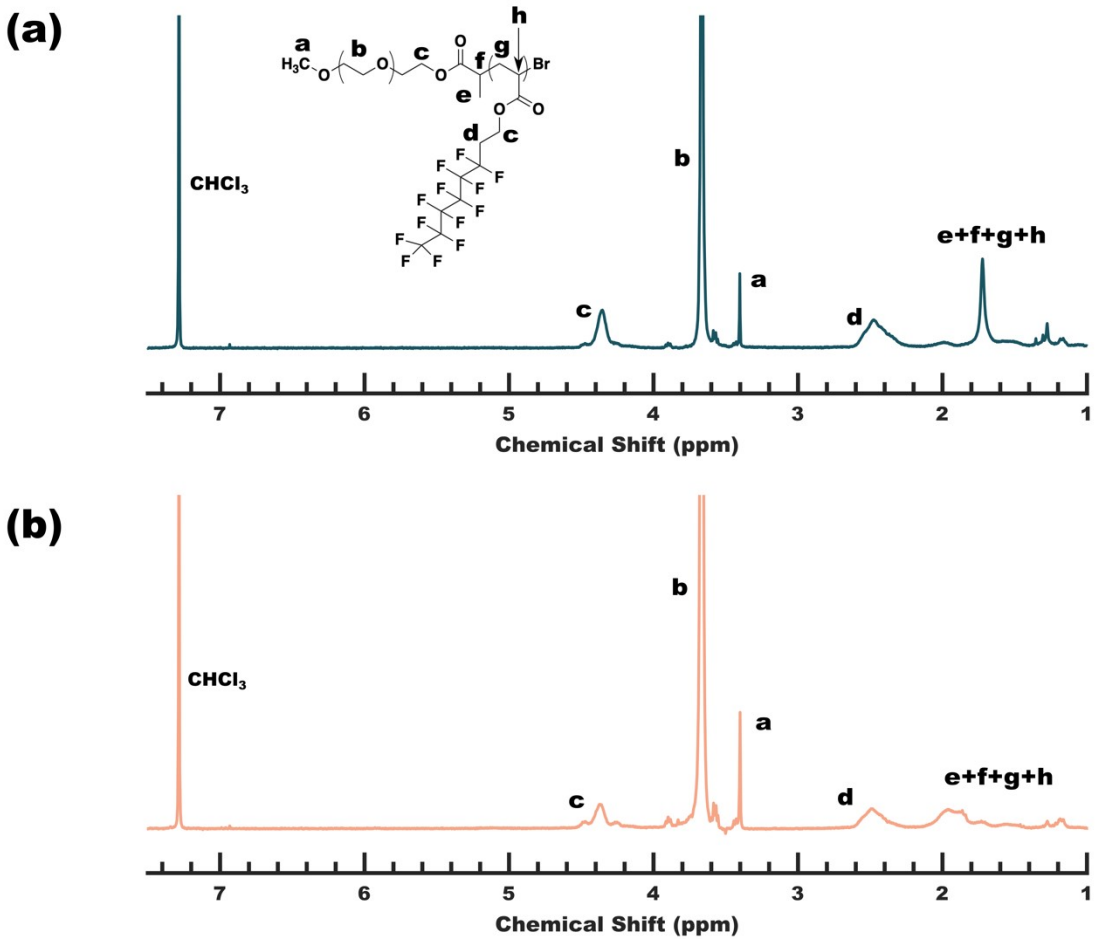

Figure S1. ^{1}H-NMR patterns for the polymers $O_{45}F_{11}$ (a) and $O_{45}F_{8}$ (b) in $CDCl_3$.

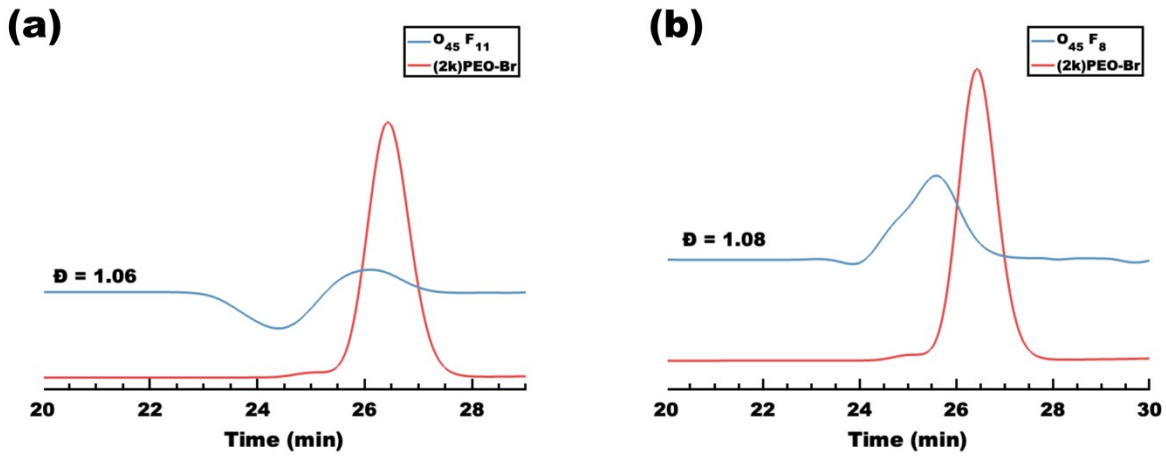

Figure S2. GPC elugrams corresponding to the synthesis of $O_{45}F_{11}$ (a) and $O_{45}F_{8}$ (b).

Table S2. ATRP Molar Ratios for the synthesis of $O_{45}F_{11}$ and $O_{45}F_8$

	$O_{45}F_{11}$	**$O_{45}F_8$**
(2k)PEO-Br	1.0	1.00
Me_6TREN	0.5	0.5
Cu(I)Br	0.5	0.5
FOA	12.0	9.0
Toluene (% sol'n. Vol.)	72.9	77.6
Temperature (ºC)	90	90
Time (hrs)	42	26

Table S3. Characteristics of the $O_{45}F_{11}$ and $O_{45}F_8$ polymers

Sample:	**M_n, PEO (g mol^{-1})**	**M_n, PFOA[a] (g mol^{-1})**	***Đ*[b]**
$O_{45}F_{11}$	2000	4600	1.06
$O_{45}F_8$	2000	3300	1.08

[a]Determined by ^{1}H-NMR [b]Determined by GPC

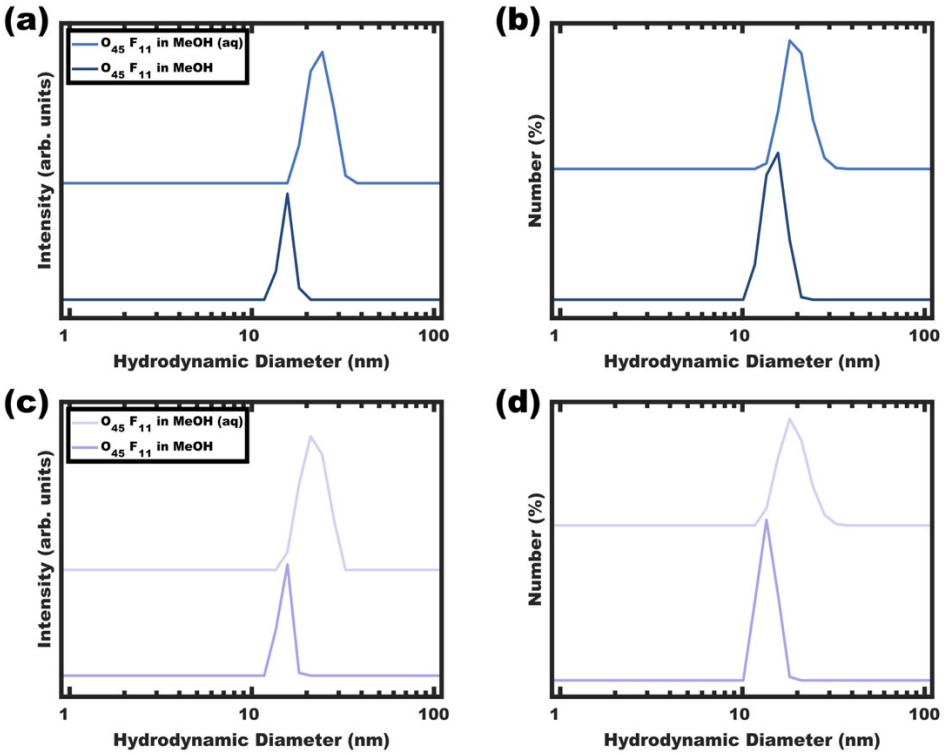

Figure S3. DLS of the $O_{45}F_{11}$ polymer before (a,c) and after (c,d) the addition of aqueous HCl either through a fast (a,b) or slow (c,d) addition rate.

Table S4. DLS hydrodynamic diameters of $O_{45}F_{11}$ micelles as a function of HCl addition rate.

Sample	Diameter in MeOH (nm)	Diameter in MeOH (aq) (nm)
$O_{45}F_{11}$ Fast Addition	**15.5 ± 0.2**	**23.9 ± 0.7**
$O_{45}F_{11}$ Slow Addition	**15.1 ± 0.1**	**22.3 ± 0.7**

Table S5. DLS size metrics for Intensity and Number plots for the $O_{45}F_{11}$ polymer in MeOH (aq).

Run	Major Intensity Value (nm)	Number Value (nm)
1	21.3 ± 0.2	19.2 ± 0.1
2	22.3 ± 0.1	21.5 ± 0.1
3	24.2 ± 0.1	21.7 ± 0.2
4	26.8 ± 0.2	20.9 ± 0.1
5	25.6 ± 0.2	21.6 ± 0.1
6	24.7 ± 0.1	23.0 ± 0.1
Average	**24.2 ± 0.2**	**21.3 ± 0.1**

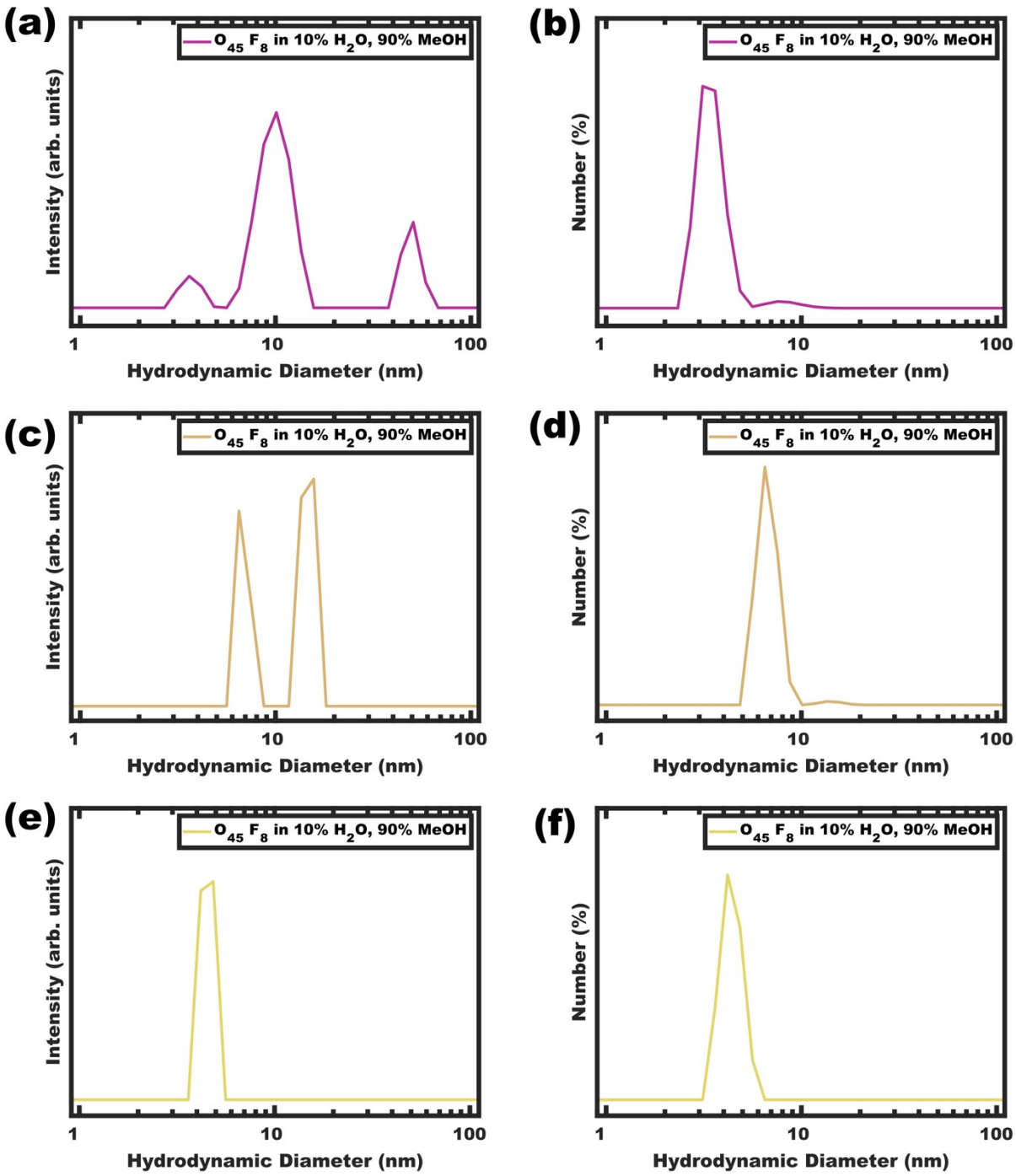

Figure S4. Repeated DLS datasets presented as intensity (a,c,e) and number (b,d,f) distributions for $O_{45}F_8$ micelles in 10 vol% H_2O, 90 vol% MeOH.

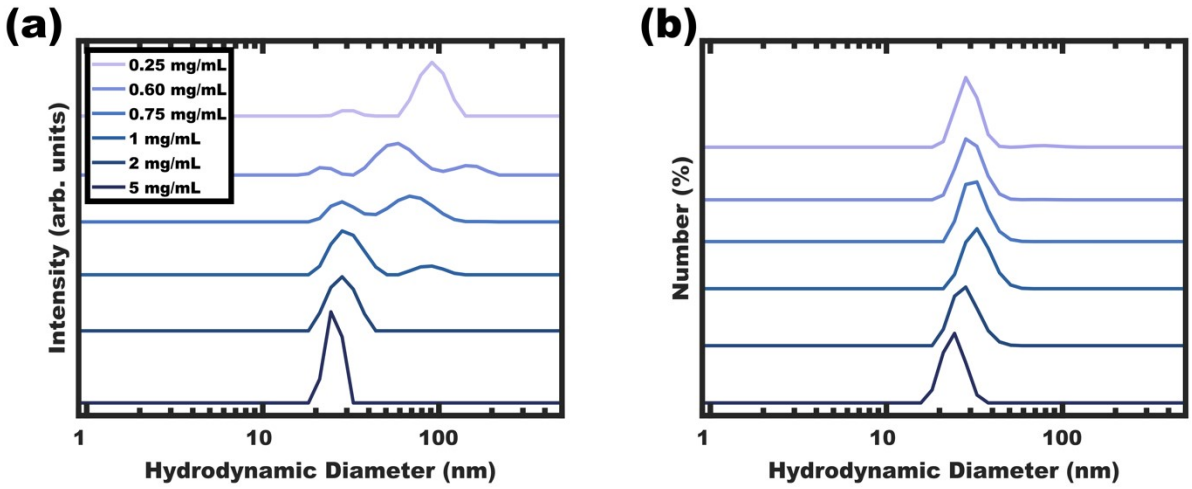

Figure S5. DLS of the $O_{45}F_{11}$ polymer at various concentrations in MeOH (aq).

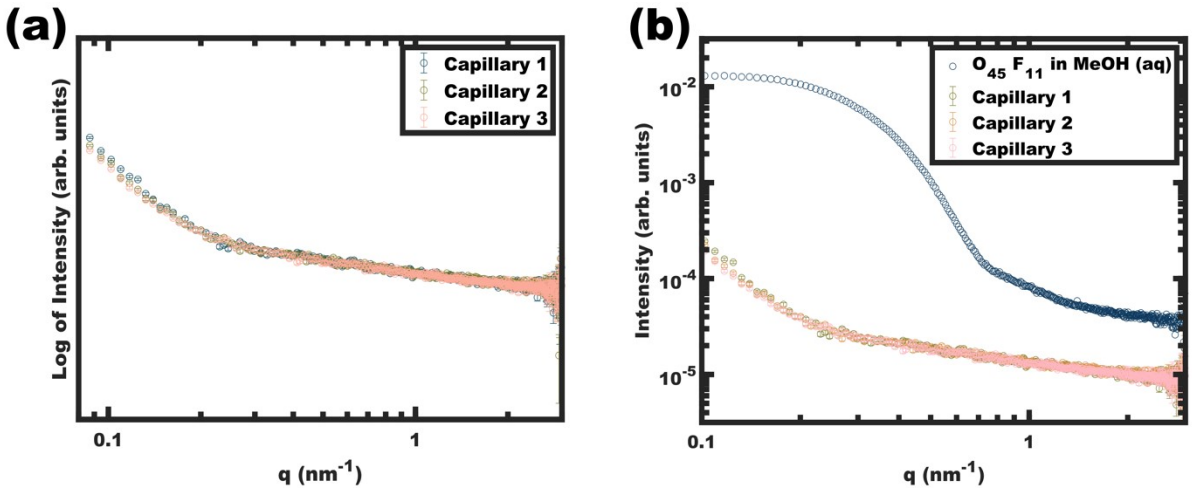

Figure S6. SAXS of multiple empty glass capillaries showing consistent background signal (a) that is several orders of magnitude weaker than the sample scattering magnitude (b).

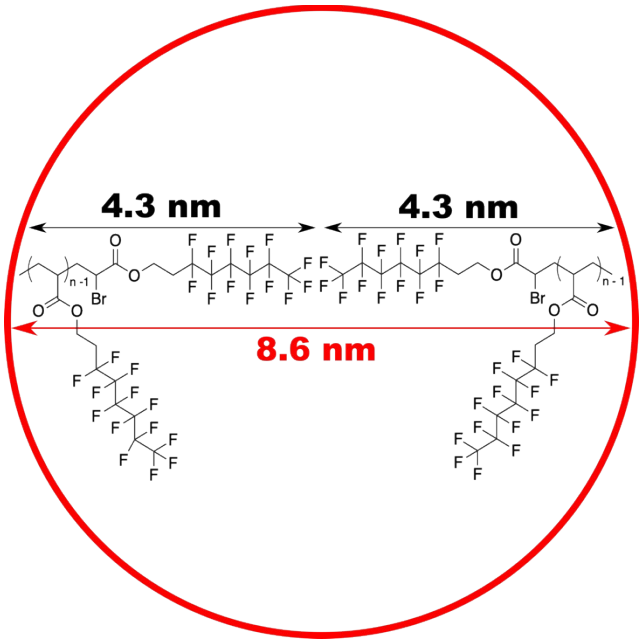

Figure S7. The maximum micelle core diameter was estimated for the PFOA micelle cores from $O_{45}F_{11}$. The contour length for F_{11} was calculated using the trans conformation. This included the 11 repeat acrylate units along the backbone (1.54 Å*cos(35.3º)*22 = 27.7 Å). The calculation also included an extended terminal FOA mer unit. The helical conformation of the extended fluoropolymers was previously reported to have 2.595 Å for each (-CF_2-CF_2-) unit,[1] i.e., ~1.30 Å per (-CF_2-) unit. The terminal FOA conformation was approximated using this value (11*1.30 Å = 14.3 Å). Half of the reported[2] 1.5 Å spacing between neighboring fluorines (-F F-) was included in the contour length calculation. Thus, the overall contour length was estimated as 27.7 Å + 14.3 Å + 1.5 Å/2 = 42.75 Å.

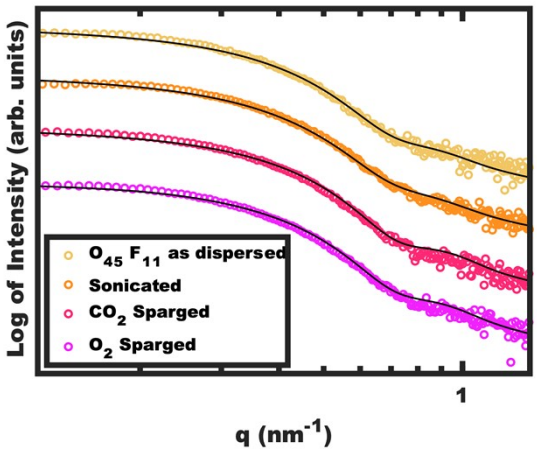

Figure S8. SAXS data for $O_{45}F_{11}$ micelles plotted in both I vs q (a) and Iq^4 vs q (b) coordinate spaces. The data were obtained from a 20 mg mL^{-1} $O_{45}F_{11}$ solution in MeOH. The data were background subtracted from a MeOH capillary blank and are offset vertically for visual clarity.

Table S6. The best-fit values for SAXS measurements on 10 mg mL^{-1} solutions of $O_{45}F_{11}$ micelles in MeOH as a function of different treatments.

Treatment	Diameter by SAXS Fitting (nm)[1]
As-dispersed	10.90 ± 0.02
Freeze-pump thaw	10.36 ± 0.01
Sonicated	10.69 ± 0.01
CO_2 Sparged	10.88 ± 0.02
O_2 Sparged	11.10 ± 0.02

[1]Confidence intervals were calculated through the minimization of residuals on the basis of the χ^2 test.

PMT Model

$$d_{spacing} = \frac{D}{2S}\sqrt[3]{\frac{4\pi}{3\gamma}}\left(x\beta + 1 + \frac{f_{corona}}{1 - f_{corona}}\right)^{1/3} \quad \text{(Equation S1)}$$

The equation for the micelle core template (MCT) model[3] assumes a constant micelle size across the series. Here, *D* represents the micelle diameter, γ accounts for unit cell distortion, *x* is the M:T ratio, β is a convolved density term,[3] and f_{corona} is the volume fraction of the hydrophilic corona-forming block (PEO). Lastly, *S* connects the structure factor peak to the SEM measured micelle-to-micelle d-spacing ($d_{m\text{-}m}$) using:

$$S = \frac{d_{m-m}}{d_{spacing}} = \frac{q\, d_{m-m}}{2\pi} \quad \text{(Equation S2)}$$

The wall thickness was deconvolved from the micelle – to – micelle spacing using the following expression:

$$w = (\alpha d_{m-m} - D) \quad \text{(Equation S3)}$$

where *w* is the wall thickness, α is a fit term that accommodates the variable distribution of wall thicknesses for different orientations, and *D* is the template/pore diameter. For a cubic crystal system, values for α are expected to range from 0.87 – 2.45 when measuring using an inscribed circle to measure wall thickness.[4]

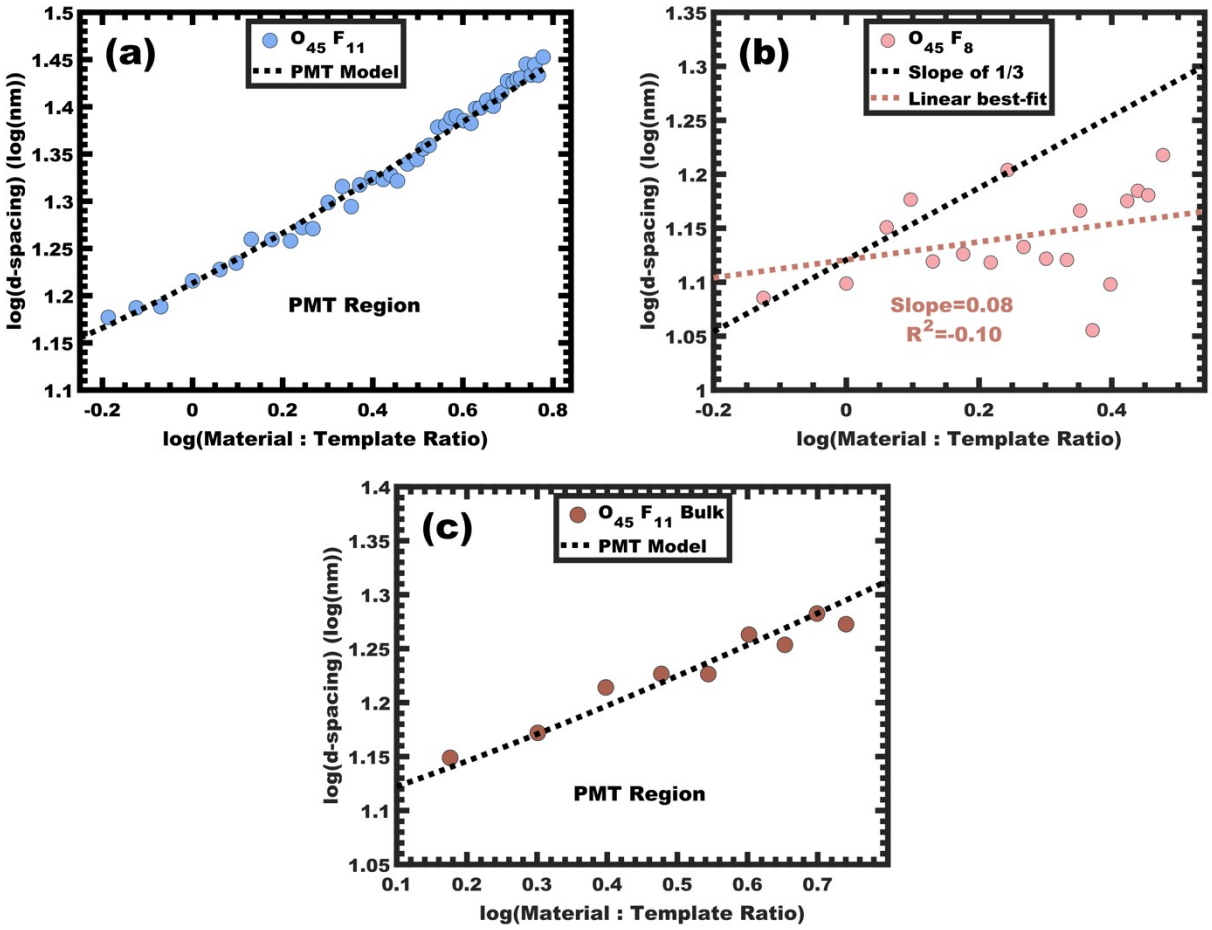

Figure S9. Thin films SAXS data from $O_{45}F_{11}$ (a), $O_{45}F_8$ (b), and bulk $O_{45}F_{11}$ (c) plotted as d-spacing vs M:T ratio in a log-log coordinate space to assess consistency with PMT trends.

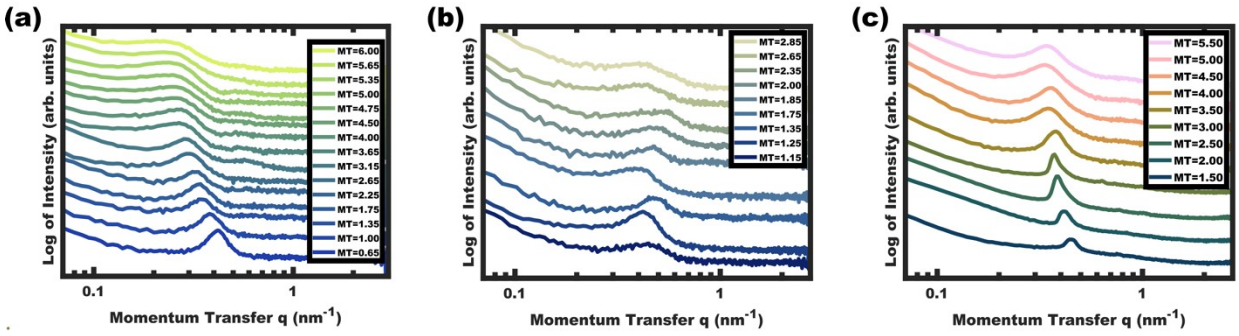

Figure S10. Log-log SAXS plots for the $O_{45}F_{11}$ thin film (a), $O_{45}F_8$ (b), and $O_{45}F_{11}$ bulk casts (c).

Table S7. SAXS d-spacing, SEM pore diameter and wall thickness data from the $O_{45}F_{11}$ thin film series. The pore size and wall thickness data are reported as the average ± the standard error-of-the-mean.

M:T Ratio	SAXS d-spacing (nm)	SEM Pore Diameter (nm)	SEM Wall Thickness (nm)
1.00	16.43	11.59 ± 0.79	4.58 ± 0.27
1.50	18.17	11.64 ± 0.70	5.37 ± 0.37
2.00	19.82	11.27 ± 0.81	6.37 ± 0.43
2.50	21.13	11.99 ± 0.82	7.71 ± 0.56
3.00	21.85	11.90 ± 0.84	7.24 ± 0.55
3.50	23.90	11.39 ± 0.85	8.34 ± 0.61
4.00	24.28	11.89 ± 0.81	9.21 ± 0.70
4.50	25.52	11.63 ± 0.83	10.58 ± 0.76
5.00	26.75	11.83 ± 0.82	10.51 ± 0.74
5.50	27.89	11.62 ± 0.76	11.06 ± 0.76
6.00	28.35	11.75 ± 0.86	12.40 ± 1.00

Table S8. Table of PMT fit parameters for $O_{45}F_{11}$ thin film and bulk cast series.

	$O_{45}F_{11}$ Thin Films	$O_{45}F_{11}$ Bulk Casts
α[a]	0.88	0.98
β[a]	3.97	2.17
γ	1.00	1.00
f_{PEO}[b]	0.38	0.38
S	1.00	1.00
Pore/Template Diameter[c]	11.68 nm[d]	10.36 nm

[a]Determined from least squares fitting analysis within the PMT window
[b]Determined from NMR analysis of polymer
[c]Determined from SEM pore size measurements within the PMT window
[d]The in-plane dimensions was used for modelling

Table S9. SAXS d-spacing, SEM pore size and wall thickness data from the $O_{45}F_{11}$ bulk cast series. The pore size and wall thickness data are reported as the average ± the standard error-of-the-mean.

M:T Ratio	SAXS d-spacing (nm)	SEM Pore Diameter (nm)	SEM Wall Thickness (nm)
1.50	14.09	10.98 ± 0.70	4.18 ± 0.34
2.00	14.86	10.06 ± 0.68	4.62 ± 0.42
3.00	16.37	10.03 ± 0.67	5.48 ± 0.36
3.50	16.85	10.88 ± 0.79	6.10 ± 0.47
4.00	18.32	9.98 ± 0.69	7.19 ± 0.61
5.00	19.17	10.14 ± 0.79	8.62 ± 0.71

Derivation of the SAXS d-spacing deconvolution model:

The pore volume from thin films was related to the parent micelles by quantifying evaporative distortions. The initially spherical micelles pack into an arrangement (Fig S7a). As the material precursors begin to cross-link, the solvent continues to evaporate, compressing both the micelle templates and the distorted lattice (Fig S7b). The micelle compression (r_{in}/r_{out}) was assumed to be equal to the lattice compression (a_{in}/a_{out}). The Fourier transform of this real-space arrangement yields reciprocal ratios of lattice parameters where $b_{out}/b_{in} = a_{in}/a_{out}$ (Fig S7d). The 3D ellipsoidal structure factor in Fourier space has a major radius q_{out} and a minor radius q_{in}, corresponding to the out-of-plane and in-plane orientations, respectively. These q values are proportional to the respective lattice parameters where $b_{out}/b_{in} = q_{out}/q_{in}$. When the sample is rotated to θ = 45º with respect to the detector then the corresponding plane of reciprocal space is measured (Fig S7e). The intersection of this plane with the structure factor is drawn from an edge-on view in Fig S7f where the largest value q_t contains both in-plane and out-of-plane contributions. The purely out-of-plane contributions are next extracted from this information.

The equation for such an ellipsoid is:

$$\frac{y^2}{{q_{out}}^2} + \frac{x^2}{{q_{in}}^2} = 1 \qquad \text{(Equation S4)}$$

The observed ellipsoid on the detector can be related to q_{out} and q_{in} by relation to q_t using an inscribed triangle and Pythagorean's theorem. The (x,y) coordinates of q_t have x = y owing to the 45º - 45º - 90º triangle where also

$$x^2 + y^2 = {q_t}^2$$

This simplifies to

$$x = y = \frac{q_t}{\sqrt{2}}$$

Thus, the q_t coordinates are $\left(\frac{q_t}{\sqrt{2}}, \frac{q_t}{\sqrt{2}}\right)$. Combining this known point with the directly measured q_{in} value allows for q_{out} to be solved for using Equation S1:

$$\frac{\left(\frac{q_t}{\sqrt{2}}\right)^2}{{q_{in}}^2} + \frac{\left(\frac{q_t}{\sqrt{2}}\right)^2}{{q_{out}}^2} = 1$$

Simplification of this yields …

$$q_{out} = \frac{q_t}{\sqrt{2 - \frac{{q_t}^2}{{q_{in}}^2}}} \qquad \text{(Equation S5)}$$

The value of q_{out} was calculated using data in Figure S8, leading to an average ratio of:

$$\frac{q_{out}}{q_{in}} = 0.719$$

This is combined with the above statements of equality to yield:

$$q_{out}/q_{in} = b_{out}/b_{in} = a_{in}/a_{out} = r_{in}/r_{out} = 0.719$$

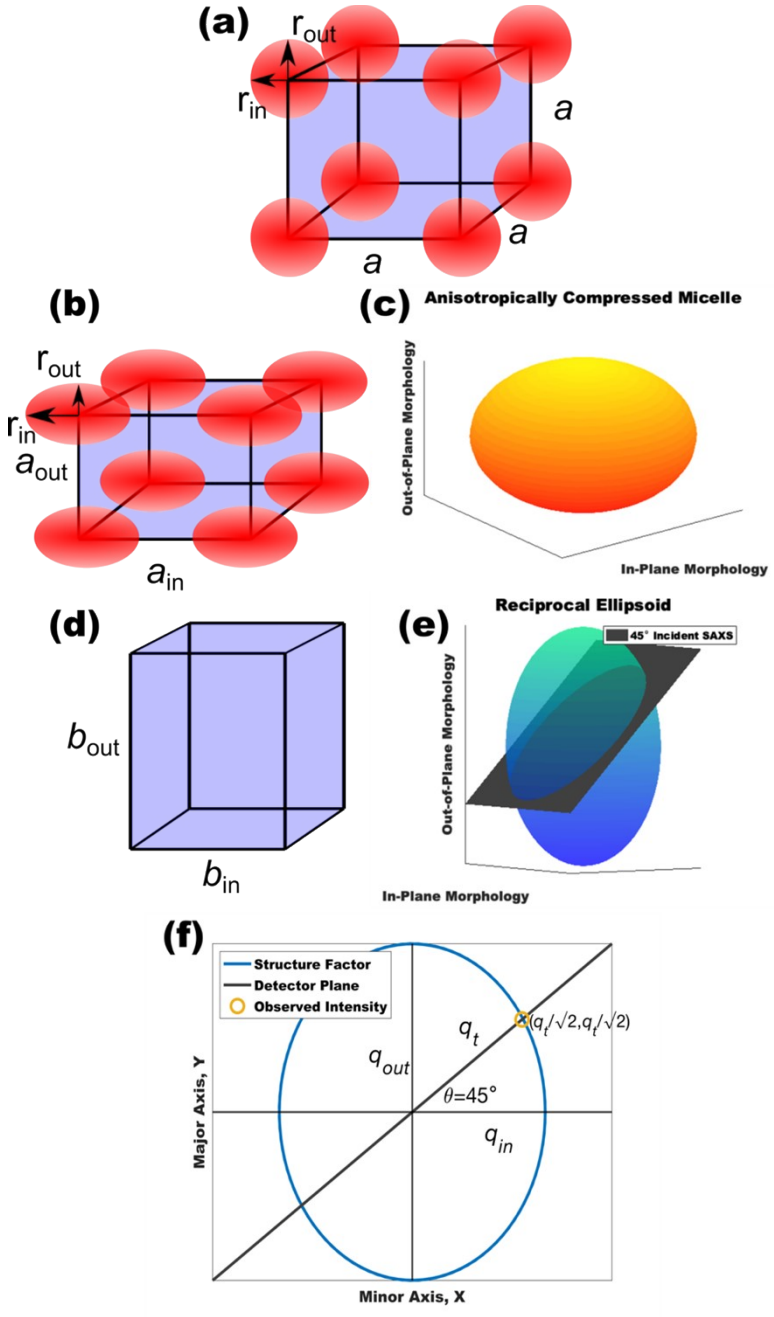

Figure S11. Representation of micelle core (material pore) character throughout the material processing timeline. A non-distorted lattice of micelle cores (red) amongst the material/corona phase (blue) is considered. During the drying process, anisotropic evaporation and substrate adhesion leads to anisotropic compression of both the lattice (b) and the corresponding micelle core (c). The corresponding reciprocal space lattice has inverse anisotropy (d). The first diffraction ring is considered in this 3D Fourier space where the detector is oriented at 45 degrees relative to the sample plane (e) to evaluate geometrical considerations of incident X-rays upon such a pore geometry (e). A side-view of the detector plane in 2D is presented to relate the observed q-value to the sample distortion.

Table S10. Comparison of micelle volume throughout materials processing

	Micelle Core Diameter/Diameters (nm)	**Core Volume (nm^3)**	**Aggregation Number** [b]	**Equivalent Undistorted Core Diameter (nm)**
$O_{45}F_{11}$ Micelle Templates in MeOH (aq)	11.24 ± 0.01 [a]	743.5 ± 2.0	109 ± 0.2[e]	11.24 ± 0.01
Porous $O_{45}F_{11}$ Thin Films	11.68 ± 0.24[b] and 8.40 ± 0.17[c]	600.0 ± 73.9[d]		10.46 ± 0.21[f]
Porous $O_{45}F_{11}$ Bulk Casts	10.35 ± 0.72[b]	580.5 ± 121.1		10.35 ± 0.72

[a]Determined from micelle SAXS form factor fitting
[b]The pore radius (mean ± standard error-of-the-mean) from analysis of SEM images
[c]Distorted minor radius estimated by dividing the SEM major radius by the SAXS structure factor compression ratio (average IP-to-OP d-spacing ratio)
[d]Calculated using the adjusted volume of an ellipse expression (Equation S4)
[e]Determined by dividing the core volume by the estimated F_{11} chain volume of 5.51 nm^3
[f]Calculated as the sphere diameter giving the same volume as the corresponding ellipsoidal core volume

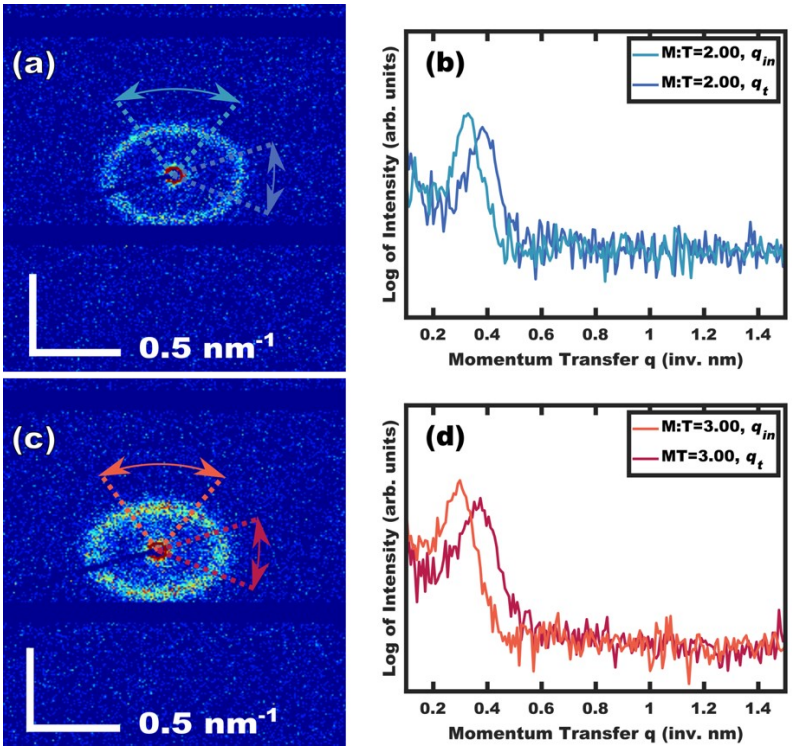

Figure S12. 2D SAXS patterns acquired with the incident beam at 45º relative to the sample plane (a, c). Wedge integrals were calculated along the major and minor directions to measure q_t and q_{in} respectively (b, d).

1 C. W. Bunn and E. R. Howells, *Nature,* 1954, **174**, 549-551.

2 L. O. Brockway, *J. Am. Chem. Soc.,* 1938, **60**, 1348-1349.

3 A. Sarkar and M. Stefik, *J. Mater. Chem. A,* 2017, **5**, 11840-11853.

4 K. A. Lantz, N. B. Clamp, W. van den Bergh, A. Sarkar and M. Stefik, *Small,* 2019, **15**, 1900393-1900403.